Estimating the Genetic Parameters of Flowering-Time Related traits in a Miscanthus Sinensis population tested with a staggered-start design

Wei HOU
BioEcoAgro Cross-border: Transfrontaliere BioEcoAgro
Raphaël RAVERDY
BioEcoAgro Cross-border: Transfrontaliere BioEcoAgro
Emilie MIGNOT
BioEcoAgro Cross-border: Transfrontaliere BioEcoAgro
Stéphanie ARNOULT
BioEcoAgro Cross-border: Transfrontaliere BioEcoAgro
Catherine GIAUFFRET
BioEcoAgro Cross-border: Transfrontaliere BioEcoAgro
Maryse BRANCOURT-HULMEL (Maryse.Hulmel@inrae.fr)
BioEcoAgro Cross-border: Transfrontaliere BioEcoAgro https://orcid.org/0000-0002-8679-7537

Research Article

Keywords: Biomass crop, Heritability, Earliness, Year effect, Climate effect

Posted Date: May 6th, 2021

DOI: https://doi.org/10.21203/rs.3.rs-466204/v1

Abstract

There is a growing interest in the cultivation of miscanthus on marginal land, but biomass yields are much lower there than on good farming land. Therefore, understanding what causes such instability is of primary interest for breeding later-flowering but stable miscanthus genotypes. Our objectives were to estimate the genetic parameters -genetic variance and genetic heritability- and genetic correlations for flowering-time-related traits in a biparental *Miscanthus sinensis* diploid population, and to divide the year effect into both age and climate effects using a staggered-start design. The population was established with single plants organized in a staggered-start design and consisted of two genotype groups established twice, in 2014 and 2015, with a total of 159 genotypes and 82 common genotypes between the two groups. All plants were extensively phenotyped for different panicle and anther emergence traits in 2018 and 2019. All traits were delayed by about 20 days in 2019 compared to 2018, which was explained by climatic conditions that occurred before the floral transition, mainly by a 3°C decrease in maximal and minimal temperatures. When dividing the year interaction effect, the genotype × climate interaction was much higher than the genotype × age interaction. The climate effect not only caused a delay in the flowering time but also involved differential genotype behavior through climate × genotype interactions, which increased the corresponding genotype × climate interaction variance compared to the genotype × age interaction variance: the climate effect decreased the genetic parameters for all flowering-time related traits, up to 20 % for broad-sense heritability. Interestingly, all traits responded similarly to the climate effect, excepting the interval between the start of panicle emergence and that of anther appearance, for which the correlation coefficients were lower due to significant climate interactions, compared to genotype × age interactions. Therefore, *M. sinensis* breeding for flowering-time related traits must be conducted under contrasted climates in order to select more stable genotypes.

Introduction

Biomass is expected to play a major role in the energy transition, which involves switching to a safe and sustainable low-carbon economy, in order to address the growing challenges due to depleting fossil resources and climate change [1]. In their review, Gabrielle et al. [1] reported that a small proportion of European renewable energy is derived from dedicated bioenergy crops. Most of them are perennials grown to generate electricity and heating, with the most frequent species being miscanthus, willow, reed canary grass, and poplar. In addition, some biomass crops are exploited in response to environmental pollution [2].

Miscanthus is a perennial C4 rhizomatous grass originating from eastern and southern Asia [3]. Notably, *Miscanthus × giganteus* was introduced in the 1930s in Europe from Japan by the Danish nurseryman, Aksel Olsen [4], and is known as a natural interspecific hybrid between *Miscanthus sacchariflorus* and *Miscanthus sinensis* [5]. Miscanthus cropping relies on *M. × giganteus* clones and has thus been used since 1983 [6]. It was rapidly identified as providing promising lignocellulosic biomass due to its high biomass yield per area [3], low nitrogen needs [7] and capability to recycle its nitrogen [8]. However, *M. × giganteus* is sterile and presents genetic uniformity. This crop currently relies on a single clone, which may cause risks that have been recognized in case of disease, pest, or climate pressure [9]. As early as 1997, Greef et al. [10] reported that genetic diversity was very low within a pool of 31 European *M. × giganteus* accessions [11]. concluded that 27 American and 6 European accessions were derived from a single clone by vegetative propagation. In contrast, *M. sinensis* exhibits huge genetic variability, with major genetic groups originating from Asia [3, 12, 13], which offers numerous opportunities to enlarge the varietal offer.

To produce biomass, crops require the longest possible vegetative growth period because the shift from vegetative to reproductive growth prevents or stops biomass accumulation. This shift is of particular interest on marginal land where biomass yields are very often much lower than on good agricultural land, and where Wagner et al. [14] found that economic sustainability is limited by the biomass yield. In miscanthus, several previous studies using different miscanthus germplasm found that late-flowering was associated with higher biomass production. Zub et al. [15] compared *M. sinensis*, *M. sacchariflorus*, and *M. × giganteus* and showed that the latest-flowering genotypes produced more biomass than the

earliest-flowering ones. Clifton-Brown and Lewandowski [16] observed that some non-hybrid genotypes of *M. sinensis* had shorter growing seasons and lower plant heights due to their earlier flowering, and their biomass yields were generally lower than those of later-flowering hybrids. Regarding the flowering diversity of miscanthus, Jensen et al. [17] compared 244 genotypes of two miscanthus species (*M. sinensis*, *M. sacchariflorus*) and 8 inter-specific hybrids including *M. × giganteus*. They found that *M. sinensis* clones were the earliest ones to flower, but showed the greatest diversity in terms of flowering onset, which highlights the importance of this species for breeding new varieties. It also shows the need for new late-flowering *M. sinensis* to increase their biomass production.

The genetic parameters, genetic variance and heritability of traits related to flowering time in miscanthus are essential to breed such new *M. sinensis* varieties. Slavov et al. [18] observed the date on which the first flag leaf emerged in a population of 138 *M. sinensis* plants and found that this trait was highly heritable (broad-sense heritability = 0.83). Gifford et al. [19] observed the day of the year of the heading date and 50% anthesis for two successive years in a population of 221 progenies from a cross between two *M. sinensis*, and found that these traits were highly heritable, with a broad-sense heritability of 0.80 and 0.67 for the heading date and 0.77 and 0.70 for the 50% anthesis. Dong et al. [20] estimated the broad-sense heritability of two diploid F1 *M. sinensis* populations for the date on which flowering first began (with opened florets, elongated stamens, and pollen shedding) and found high heritability levels (0.76 and 0.85). In all these studies, the flowering-related traits were limited to a single trait except in the work of the last authors who studied several traits, but only one related to flowering, *i.e.* the date on which flowering first began.

So far, the climate effect on genetic parameters has not been specifically addressed in miscanthus. In the present study, the objectives were hence to estimate the genetic parameters and genetic and phenotypic correlations for traits related to flowering, with a specific focus on the year effect. We studied a biparental diploid *M. sinensis* population using a staggered-start design [21] established twice, in 2014 and 2015, and extensively phenotyped in 2018 and 2019 for flowering-time related traits. The power of such a design in which the population was established twice makes it possible to divide the “growing year” effect into “age” effect and “climate” effects [22, 23]. Therefore, we paid attention to what caused the flowering-time related traits to be delayed in 2019 compared to 2018. What caused the genetic parameters to change? We predicted that the climate effect would be different from the age effect, which sheds new light on the study of genetic parameters and correlations in *M. sinensis.*

Materials And Methods

Trial conditions and experimental design

The field trial was established in 2014 at the INRAE unit in Estrées-Mons (49° 72’ N, 3° 00’ E) in northern France, relying on the frame of the Biomass For the Future (BFF) project. It was repeated twice in 2014 and in 2015 using a staggered-start design [21]. The field soil type was characterized as deep loam (Ortic luvisol, FAO, classification). The trial received no nitrogen input and weeds were regularly manually removed. Meteorological data were recorded daily at a short distance from the trial (about 1 km) and downloaded from the CLIMATIC database (INRAE AGROCLIM, 2020).

Population and experimental design

The population consisted of the F1 progeny of 159 individuals generated from an intraspecific cross between two diploid *M. sinensis* varieties, “Silberspinne” and “Malepartus”. Plantlets were initially produced from the seeds and grown in a greenhouse in order to provide clonal replicates of each genotype using *in vitro* propagation method [24]. The population was established with single plants organized in a staggered-start design [23]. An initial group of genotypes (coded G1), that contained a total of 111 genotypes and included the two parents, was established in 2014 using an initial incomplete block design [25]. A second group of 130 genotypes (coded G2) included the two parents as well and was established in 2015 using a second incomplete block design. 82 genotypes were common to both groups and established twice in 2014 and 2015 to allow the partition of the year effect into age and climate effects. The staggered-start design comprised a total of

1155 plants. Each established group comprised 5 blocks of 90 individuals each (6 rows of 15 plants each). The two parents were grown in each block while the G1 remaining genotypes were randomly spread into four blocks on average and the G2 genotypes into at least three blocks. The two groups of genotypes, which were adjacent in the field, were separated using 75 plants (15 x 5) and surrounded by 180 border plants, to guarantee similar competition effects. Individuals were randomly planted using the Excel package « BICA » wh,ich was based on VBA programming language and developed for the randomization of incomplete blocks (JC Bastien, personal communication). A density of 1 plant/m² was applied at regular intervals of 1 m × 1 m between the plants.

Phenotyping of traits related to flowering

The phenotypic observation of the individuals within the population for flowering-related traits was conducted in 2018 and 2019. The following traits were recorded on each plant and targeted stems belonging to the higher part of the plant canopy (above 80%): the start of panicle emergence (SPE), which corresponds to the date on which the first panicle was visible at least 1 cm above the plant stem; anther appearance (AA), which corresponds to the date on which anthers appeared and began to shed pollen -this observation was carried out on the first panicle that emerged in the plant; the mid-point panicle emergence (MPE), which corresponds to the date on which 50% of the panicles had emerged in the plant, and finally, the complete panicle emergence (CPE), which corresponds to the date on which over 80% of the panicles of the entire plant had emerged. In addition, one variable was calculated: the interval between heading and flowering (IHF) that was defined as the difference between the heading and flowering dates observed on the first panicle that emerged and flowered. To reduce bias and increase accuracy in the data To guarantee data accuracy, phenotypic observations of the traits were made three times a week, starting with the first plant that showed panicle emergence. The first panicle to appear on the plant was marked and used for further determination of the date of anther appearance to facilitate determination and avoid sampling bias. In addition, other traits were observed in the population: the emergence date (ED), the senescence date (SD) that corresponded to the date on which the first stem cohort had become completely senescent, and the date of the first winter frost (FD).

To further calculate weather indicators, extensive observations were conducted on Malepartus, one of the two population parents, in order to determine the date of the floral transition. This clone was established in 2014 in a specific trial not far from the population trial, at a plant density of 2 plants/m² (see Leroy et al., submitted to BioEnergy research). The sampling was carried out on three plots of about 75 m² each. The floral transition corresponded to the differentiation of the terminal vegetative apex into a panicle and was observed by dissecting 30 apices per day on average from May 24th onwards. It was determined as the date of the first floral transition appearance, which was expected to correspond to the floral transition of the first stem that showed a panicle above the canopy.

Based on previous results obtained in maize, leaf appearance rate and duration responded to temperature in approximately the same way as for primordia and were constant across temperature regimes, at least for the appearance of the first 12 leaves [26]. According to Hesketh and Warrington [27], the use of a degree-day model must predict the appearance rate of new organs, such as leaf primordia, tassel, and ears, as a function of air temperature or degree days. These results relating to constant degree-day durations were applied here in miscanthus to predict floral transition (referring to leaf primordia results in maize) and flowering (referring to tassel and ear results in maize). We found that the sum of temperatures calculated from emergence to flowering for the Malepartus clone with a base temperature between 6 and 8.5°C were almost equal in 2018 and 2019 when the base temperature used was of 8°C. This meant that the base temperature was close to 8°C for Malepartus and could be applied for further calculations. Therefore, growing-degree days (GDD) were estimated using 8°C as a base temperature for Malepartus and its offspring. Using the floral transition date determined from the apices observations in Malepartus, the ratio between the GDD for the emergence-to-floral transition period and the GDD for the emergence-to-flowering period was calculated for Malepartus in 2018 and reached 0.17. This ratio was then applied to the population in order to estimate floral transition dates based on flowering date observations.

Determination of plant growth periods

Five periods of the plant cycle were taken into account to calculate the weather indicators (Table 1). The first period corresponded to the pre-emergence phase (coded Period 1) and the calculations started at senescence, which occurs in the autumn, and precedes shoot emergence. The second period (Period 2) started with shoot emergence and ended with floral transition. The third period (Period 3) corresponded to the interval between floral transition and anthesis. The fourth period (Period 4) was from anthesis to senescence. Lastly, the fifth period (Period 5) covered the duration from senescence to the date of the first winter frost, the plant cycle being stopped by the first frosts.

Table 1 Description of the periods used for the weather indicator calculations. The dividing point of the growth stages was determined by mean Malepartus growth stages.

Period	Description	Year	Beginning	Ending	Duration
Period 1	Pre-emergence from the senescence of the year (n-1) to emergence year (n)	2018	324	97	138
		2019	289	81	157
Period 2	Emergence to beginning of floral transition	2018	98	134	36
		2019	82	147	65
Period 3	Beginning of floral transition to beginning of anthesis	2018	135	204	69
		2019	148	228	80
Period 4	Beginning of anthesis to senescence	2018	205	288	83
		2019	229	327	98
Period 5	Senescence to the date of frost day of the year	2018	289	346	57
		2019	328	337	9

Weather indicator description

In order to explain the climate effect, the following meteorological indicators were determined: air minimum temperature (MinT), air maximum temperature (MaxT), air mean temperature (MeanT), soil minimum temperature (MinTs), precipitation (Prec), cumulated precipitation (Prec_S), mean humidity (MeanH), vapour pressure deficit (VPD), maximum VPD (VPD_M), Penman evapotranspiration (ETPP), photosynthetically active radiation (PAR), cumulated growing degree-days (CGDD). The summary of the meteorological indicators per growing period over the two years is shown in table 2.

Table 2 The mean value of weather indicators in five growth periods in 2018 and 2019.

Weather indicator	Period 1		Period 2		Period 3		Period 4		Period 5	
	2018	2019	2018	2019	2018	2019	2018	2019	2018	2019
Prec_S/mm	312.5	327.5	26.0	54.5	136.5	112.5	126.5	208.5	116.5	21.5
Prec/mm	2.25	2.09	1.08	0.97	1.64	1.22	1.38	2.11	2.38	2.39
MeanH/mm	88.5	87.5	75.4	72.1	72.0	72.1	73.3	81.4	89.8	91.4
MinTs/℃	4.1	5.6	11.9	9.5	18.1	18.1	16.7	13.1	7.3	6.6
MinT/℃	2.3	3.5	8.2	5.2	12.2	12.2	11.6	9.0	4.8	4.2
MaxT/℃	7.8	9.6	18.3	15.3	23.8	24.0	23.1	17.4	10.4	9.1
MeanT/℃	4.8	6.3	13.1	10.1	17.9	18.0	16.9	12.9	7.4	6.5
VPD/%	0.1	0.13	0.41	0.37	0.61	0.63	0.57	0.33	0.11	0.08
VPD_M/%	0.27	0.37	1.16	1	1.66	1.74	1.64	0.96	0.31	0.23
ETPP/mm	0.63	0.57	2.88	2.81	4.27	4.42	2.84	1.78	0.38	0.23
PAR/d cm^{-2}	230.4	217.5	747.9	720.2	989.0	932.6	678.6	438.5	163.2	120.6
CGDD/d ℃	-	-	209.2	203.1	963.5	957.6	590.6	453.1	-	-

Prec_M: mean precipitation; Prec_S: accumulated precipitation; MeanH: mean humidity; MinTs: soil minimum temperature; MinT: minimum temperature; MaxT: maximum temperature; MeanT: mean temperature; VPD: vapor pressure deficit; VPD_M: maximum VPD; ETPP: Penman evapotranspiration; PAR: photosynthetically active radiation; CGDD: cumulated growing degree-days.

Statistical analyses

Two different analyses for unbalanced datasets were performed, according to the “age” effect and the “climate” effect models (Fig. 1). 159 genotypes were included in each of these analyses, with 82 in common between the G1 and G2 genotype groups.

An initial round of analyses of Linear Mixed Models consisted of a full statistical model which took into account block and spatial effects using the “breedR” package implemented in the R software [28]. It accounted for the environment heterogeneity within each trial among the blocks and diagnosed spatially distributed patterns of remaining residual variations using variograms. All variance components of the progeny were estimated by using the remlf90 function of the package, based on restricted maximum likelihood estimations. The equation of Model 1 was as follows:

$$Y_{ijkl} = \mu + \alpha_i + \beta_j + (\alpha\beta)_{ij} + \delta_l + \varepsilon_{ijkl}$$

where Yijkl represents the phenotypic value measured on plant k of genotype i at age j in block l; μ is the overall mean; αi is the random effect of genotype i; βj is the fixed effect of age j; (αβ)ij is the random interaction between genotype i and age j; δl is the effect of block l and εijkl is the random residual for plant k of genotype i at age j in block l. An autoregressive spatial component was also considered in the model based on x and y coordinates in each plot in order to partition the residual εijkl into a spatially dependent parameter, θikl, for plant k of genotype i in block l, and an independent remaining residual [29].

This full model was compared with two sub-models for each trait: a sub-model with no decomposition of the residual term into spatially dependent and independent effects and another sub-model with no block effect but with the decomposition of

the residual term into spatially dependent and independent effects. The performance of the three models was compared on their Akaike information criterion, for which a lower value corresponded to a better performance. For all traits, the last sub-model, which dropped the block effect but took into account the spatial effect, was found to have a slightly better performance than the full model or than the sub-model which dropped the spatial effect but took into account the block effect. Accordingly, it was retained afterwards, which simplified the models.

The “age” effect was assessed using the following Linear Mixed Model, fitted for each studied trait and considering each year in which the progeny grew. It was referred to as “age effect model”:

$$Y_{ijk} = \mu + \alpha_i + \beta_j + (\alpha\beta)_{ij} + \theta_{ik} + \varepsilon_{ijk} \quad (1)$$

where Y_{ijk} represents the phenotypic value measured on the plant k of genotype i at age j, μ is the overall mean; α_i is the random effect of the genotype i; β_j is the fixed effect of age j; $(\alpha\beta)_{ij}$ is the random interaction between genotype i and age j; θ_{ik} is the random spatial effect for plant k of genotype i; and ε_{ijk} is the random residual error for plant k of genotype i at age j. This modeling was carried out by using two subsets of the data (rectangles colored in blue in Fig. 1). The year 2018 was considered for G1 and G2 and the age effect was taken into account by 4-year old plants with G1 and 3-year old with G2. Plants of different ages grew in the same climate during a same year (2018), which makes it possible to take into account the age effect in the same climate conditions. The age effect was also analyzed in 2019 in the same manner when the genotypes were one year older.

The performance of the full model including the interaction term was compared with the corresponding sub-model with no interaction by using the Akaike information criterion. Based on the AIC, the analysis showed that a model that included interaction effect was always more performant than the sub-model for all traits.

Then, the “climate” effect was assessed using the following Linear Mixed Model, for each age of the progeny. It was referred to as “climate effect model”:

$$Y_{ilk} = \mu' + \alpha'_i + \gamma_l + (\alpha'\gamma)_{il} + \theta'_{ik} + \varepsilon'_{ilk} \quad (2)$$

where each term is similar to model (1), except that the age effect β_j is replaced by γ_l, the climate effect of year l and the interaction between genotype i and age j by the interaction between genotype i and climate l . It can be noted that the spatial effect term was a different estimate in comparison to the estimate from model 1. In this modeling, only 4-year old plants were considered and corresponded to G1 genotypes which grew in 2018 and G2 genotypes in 2019 (orange rectangle in Fig. 1). Plants of the same age grew in two different climate conditions, related to each year considered. The performance of the full model including the interaction term was tested in the same manner as previously and the results showed a higher performance of the model that included interaction effect for all traits.

According to these two models, genotypic broad-sense heritability was estimated as follows:

- For the age effect,

$$H^2_{sl} = \frac{\sigma^2_{\alpha}}{\sigma^2_{\alpha}+\sigma^2_{\alpha\beta}+\sigma^2_{\theta}+\sigma^2_{\varepsilon}} \quad (3)$$

where σ^2_{α} is the variance attributed to the genotype, $\sigma^2_{\alpha\beta}$ is the variance of the genotype × age interaction, σ^2_{θ} is the spatial variance and is σ^2_{ε} the residual variance.

- For the climate effect,

$$H^2_{sl} = \frac{\sigma^2_\alpha}{\sigma^2_\alpha + \sigma^2_{\alpha\gamma} + \sigma^2_\theta + \sigma^2_\varepsilon} \quad (4)$$

Here, each term is similar to the previous formula, except for $\sigma^2_{\alpha\gamma}$ which is the variance of the genotype × climate interaction.

According to the two previous models, progeny-mean heritability [30, 31] was also estimated for the age and climate effect models, respectively as:

$$H^2_{Pi} = \frac{\sigma^2_\alpha}{\sigma^2_\alpha + \frac{\sigma^2_{\alpha\beta}}{J} + \frac{(\sigma^2_\theta + \sigma^2_\varepsilon)}{JK}} \quad (5)$$

$$H^2_{Pi} = \frac{\sigma^2_\alpha}{\sigma^2_\alpha + \frac{\sigma^2_{\alpha\gamma}}{L} + \frac{(\sigma^2_\theta + \sigma^2_\varepsilon)}{LK}} \quad (6)$$

where J are the two ages considered, L are the two climates (of each year) and K is the mean number of repetitions per genotype.

Due to the unbalanced feature of the design, as all genotypes were not common between G1 and G2 (*i.e.* not established twice in 2014 and 2015), most previous models were applied twice as a second round of analyses was restricted to the 82 common genotypes between G1 and G2. It allowed a more precise comparison of the climate and age interaction effects, thus avoiding biases due to non-common genotypes between the comparisons.

Genetic and phenotypic correlations were then assessed for each trait, considering a given age or a given year. Genetic correlations were estimated as described by Howe et al [32]. To calculate phenotypic correlations, Pearson correlation coefficients were computed using R package “stats” and visualized using R package “corrplot” [33].

A Principal Component Analysis (PCA) was performed on the weather indicators determined in Table 2 using the R “FactoMineR” package. This PCA was followed by a clustering that was applied to the coordinates of the individuals in the two first components of the PCA. These individuals corresponded to combinations between the periods and the two years. Within a period, the number of clusters was defined when the two years of a given period were separated. Then, the climatic features of the separated combinations were pointed out.

Results

A delay of about 20 days was observed in 2019 compared to 2018 for all flowering-time related traits

When comparing the two years of observation, the flowering time was significantly delayed - by around 20 days on average - in 2019 in comparison to 2018 (Table 3). In 2018, the median DOY values for the start of spike emergence (SPE), anther appearance (AA), mid-point of spike emergence (MPE), and completion of spike emergence (CPE) were 212, 218, 218, and 222, respectively. In 2019, the median DOY values for SPE, AA, MPE, and CPE were all delayed to 233, 238, 239, and 243, respectively. After discarding extreme odd values (corresponding to a 95% interval from 2.5–97.5% DOY quantiles), the

range of the population was rather stable in both years for each flowering trait. It was around 30 days excepting for CPE observed in the first group of established genotypes (G1).

Table 3
DOY quantiles, mean and standard deviation calculated for all flowering-time-related traits and genotype groups in both years. Range of the population determined by the interval between 2.5–97.5%.

Trait	Genotype group	2.5% quantile		Median		97.5% quantile		Mean		S.D.		95% quantile interval	
		2018	2019	2018	2019	2018	2019	2018	2019	2018	2019	2018	2019
SPE	G1	197	218	213	235	229	246	213	234	8.1	6.1	32	28
	G2	197	214	211	232	227	245	212	231	6.6	7.5	30	31
AA	G1	201	224	218	239	234	254	218	239	8.7	5.3	33	30
	G2	203	220	218	238	234	256	218	236	7.5	7.7	31	36
MPE	G1	206	230	218	240	236	255	219	241	7.7	5.5	30	25
	G2	206	226	217	238	234	255	218	238	6.6	6.1	28	29
CPE	G1	211	233	222	244	238	259	223	244	7.6	5.7	27	26
	G2	208	230	222	242	238	259	222	242	6.7	6.2	30	29
IHF	G1	2.0	1.0	5.0	4.0	13.0	13.0	5.4	5.3	2.8	2.9	-	-
	G2	2.0	1.3	5.0	5.0	14.0	13.0	6.3	5.7	3.1	2.9	-	-

The climate effect induced lower genetic parameters than the age effect

The genetic and environmental variance traits were calculated for the flowering-time related traits using the two models that were distinguished by the age and climate effects, and by the corresponding interaction effects with the genotype (models 1 and 2). These traits included SPE, AA, and MPE, CPE, and IHF (Fig. 2).

Considering the climate effect model, an initial dataset was used, which corresponded to G1 tested in 2018 and G2 in 2019 (Fig. 2a): all these plants presented the same plant age of 4 years old, but grew in different years, *i.e.* different climatic conditions, which made it possible to test the climate effect on the variance components. A second dataset was also used as it corresponded to the previous one which was restricted to the common genotypes between G1 and G2 (Fig. 2b). The results showed that genetic variance most influenced each flowering trait (Fig. 2a, b). The variance corresponding to the interaction between genotype and climate was substantial, while the residual variance was lower than the two previous ones. Therefore, the broad-sense heritability estimations for all flowering-time related traits were moderate and ranged from 0.55 to 0.62, whereas the progeny-mean heritability estimations were higher than expected, and ranged from 0.77 to 0.82. The second dataset, which was restricted to the common genotypes between G1 and G2, provided similar trends. Therefore, estimates of heritability were relatively similar for balanced designs using these common genotypes compared to the unbalanced dataset (*i.e.* the first dataset): broad-sense heritability estimations for all flowering-time related traits were moderate and ranged from 0.53 to 0.61 while the progeny-mean heritability estimations were high and varied from 0.79 to 0.85.

Regarding the age effect model, two datasets were observed: G1 (established in 2014) and G2 (established in 2015) that were observed either in 2018 (dataset corresponding to Fig. 2c) or in 2019 (dataset corresponding to Fig. 2e). G1 and G2 corresponded to the plant groups at different ages but grew during the same year. In 2018, when the plant age was 4 for G1 and 3 for G2, all flowering-time related traits showed large genetic variances but displayed small variances for the

interaction of the genotype with age, as well as for the spatial effect (Fig. 2c). Due to these small environmental component variances, the broad-sense heritability estimations for all flowering-time related traits were higher than those observed with the climate effect model and ranged from 0.73 to 0.77, while the progeny-mean heritability estimations were very high and varied from 0.9 to 0.92. As for the climate effect model, the same trend was observed when the analysis was restricted to the common genotypes as the same estimates of genetic parameters were obtained (Fig. 2d).

In 2019, older plant ages were analyzed and corresponded to plant age 5 for G1 and plant age 4 for G2 (Fig. 2e). In comparison to 2018, there was a noticeable shift in the total variance and genetic variance towards lower values while the genetic variance remained the largest contribution to the total variance. Larger interaction effects between genotype and age were also noticeable in 2019, in particular for SPE and AA. Consequently, broad-sense heritability was lower in 2019 than in 2018 and varied from 0.61 to 0.69, and so were progeny-mean heritability estimations that ranged from 0.81 to 0.83 for all flowering-time related traits.

When comparing Fig. 2a with 2c in order to better understand the difference between the climate and age effects on flowering-time related traits, the results showed that the total variance of each flowering trait was almost similar under the effects of climate and plant age (observed in 2018). For all flowering-time related traits, the interaction variance between genotype and climate (with model 2) was much higher than the interaction variance between genotype and plant age (with model 1): the climate increased these interaction variances from three to sevenfold according to the trait. The interactions between genotype and climate (on the x-axis, Fig. 3) were indeed higher than interactions between genotype and age (on the y-axis). In contrast, the spatial and residual variances were rather stable between the climate effect model and the age effect modelled in 2018. To avoid biases in these comparisons, the datasets were restricted to the common genotypes between G1 and G2 (Fig. 2b, d) and provided very similar results to those obtained from the whole datasets by comparing Fig. 2a to Fig. 2c. When comparing the climate effect model to the age effect modelled in 2019 (Fig. 2a, e), the trend was the same, although the total variance of the age effect modelled in 2019 was lower and the increase due to the climate was of a lesser extent: nevertheless, the interaction variance between the genotype and the climate for all flowering-time related traits was still higher than the interaction variance between the genotype and the age for all flowering-time related traits modelled in 2019, but increased from two to fourfold.

High positive genetic correlations where observed among most flowering-time related traits when the plant age or climate effects were modelled

Genotypic and phenotypic correlations among the flowering-time related traits were estimated using climate and age effects models (reported above and below the diagonal of Fig. 4, respectively). The results showed that the phenotypic correlation coefficients for all flowering-time related traits in all data sets were lower than the corresponding genotypic correlation coefficients, but all values coincided. Therefore, the present study focused on comparing correlations at the genetic level. The same traits as before were studied (SPE, AA, MPE, CPE, and IHF).

In 2018, the estimates found under the age effect modelling process showed strong and positive genetic correlations among SPE, AA, MPE, and CPE (Fig. 4). For instance, CPE showed the highest correlation (0.99) with MPE among these higher correlated flowering-time related traits, and the smallest correlation coefficient (0.93) was observed for AA with SPE, MPE, and CPE. IHF showed a positive and significant correlation (0.45) with AA and a positive but not significant correlation with other flowering-time related traits (0.08 to 0.18).

Similarly, in 2019, the age effect model of the population corresponded to older plants, the genetic correlation estimates remained strong among SPE, AA, MPE, and CPE. IHF showed a shift toward negative and weak values with SPE, MPE, and CPE. A positive (but not significant) correlation with AA can also be noted. In addition, the genetic correlation estimates relating to the climate model at plant age 4 also performed a very similar result as the age effect model of the population.

Comparing the genetic (above the diagonal of Fig. 4) and phenotypic (below the diagonal of Fig. 4) correlations of all traits, the result provided a very similar information, where the genetic correlation coefficient coincided with the phenotypic correlation coefficient, and the genetic correlation coefficient a little larger than the phenotypic correlation coefficient.

Climatic conditions that occurred before the floral transition contributed to the differences between the two years

Due to the previously highlighted high climate effect, a Principal Component Analysis (PCA) was conducted to identify the weather indicators that contribute to the climate effect for the flowering-time related traits observed in the F1 population. The first two principal components (PCs) accounted for a large proportion of the total variation (93.0 %), with PC1 explaining 84.2 % and PC2 explaining 8.8 %. (Fig. 5).

The PC1 first component showed that 8 weather indicators had high positive loadings (> 0.9), on the right-hand position of Fig. 5a: indicators related to temperatures (MinT, MeanT, MaxT for the air and MinTs for the soil), vapour pressure deficit (VPD and maximal VPD_M), Penman evapotranspiration (ETPP), and photosynthetically active radiation (PAR). Moreover, these indicators were highly correlated with each other. PC1 also indicated that MeanH had a high negative loading (<-0.9), on the left-hand position of Fig. 5a. PC2 was explained by a single variable that was related to the sum of precipitation calculated for each period and each year (Prec_S).

The clustering of the coordinates on the first two PCA components of the individuals (*i.e.* periods according to year) clearly divided them into seven distinct groups (Fig. 5b). Most groups included both years for the periods, excepting two periods: Period2 which corresponds to the shoot emergence to floral transition phase (determined using the Malepartus clone) and Period4 which corresponds to the flowering to senescence phase. Interestingly, Period2 gathered climatic events which preceded flowering: it can be noted that both years received little precipitation while the temperature was greater in 2018 compared to 2019. During period 2, all indicators related to temperature were higher for 2018 compared to 2019. which points to warmer weather conditions in 2018: maximum temperature of 18.3°C against 15.3 ° and minimum temperature of 8.2°C against 5.2°C. The duration of period 2 in 2018 was 35 days, which was 30 days less than the same period in 2019, but it was rather constant in both years when estimated in cumulative growing degree-days (209.2 for 2018 and 203.1 for 2019).

Discussion

In the present study, the flowering related traits were extensively phenotyped within an F1 diploid population of *M. sinensis* for two years (2018 and 2019) and included the start of spike emergence (SPE), anther appearance (AA), mid-point of spike emergence (MPE), completion of spike emergence (CPE) as well as the interval between the start of spike emergence and anther appearance (IHF). All flowering-time related traits differed significantly within the population according to the genotypes and years. Interestingly, the flowering time was significantly delayed - by around 20 days in 2019 compared to in 2018 (Table 3). A climate effect on the genetic parameters was also observed but traits responded similarly to this effect. Therefore, the discussion focused on three points: 1) the flowering time delay may be explained by climatic conditions that occurred before the floral transition, 2) the genotype × climate variances were greater than the genotype × age variances for all flowering-time related traits, which implied a decrease in heritability and, 3) although the existence of these previously significant effects of the climate, most flowering-time related traits of the population behaved similarly to changes in climatic conditions.

The delay in the flowering time was explained by climatic conditions that occurred before the floral transition

Two periods were highlighted based on an extensive analysis of weather indicators according to different periods of the plant cycle: a principal component analysis followed by a clustering of the first two component coordinates of the periods for both years showed that Period 2 and Period 4 were subjected to different weather conditions in 2018 and 2019. Period 2,

which corresponds to the shoot emergence to floral transition period, is interesting because it concerned climatic events that occurred before flowering, which may have an impact on the flowering time. In particular, cooler temperatures during the period preceding floral transition (a 3°C decrease in maximal and minimal temperatures) contributed to the 20-day delay for the flowering time between the two years. In this study, we also observed that all weather indicators for the subsequent period from floral transition to flowering were very similar in both years, especially those related to the temperature that were almost identical. Therefore, differences in the temperatures observed during the emergence to floral transition period accounted for the delay in the flowering time in 2019. A significant delay was also observed between years (including both age and climate effects) in the mean annual flowering day in *M. sinensis* [17]. Growing seasonal precipitation, degree days, and the temperature calculated for the whole growing season partially accounted for this delay. In our study, we highlighted that the period preceding flowering, and in particular the period preceding the floral transition stage is critical and has an impact on the flowering of miscanthus. Regarding cooler conditions, Clifton-Brown et al. [9] found that, in a multi-environment experiment, *M. sinensis* flowered later in the growing season at lower-temperature experimental sites. Nunn et al. [34] compared the growth of 15 miscanthus germplasm types, including *M. sinensis*, *M. sacchariflorus* and, *M. × giganteus*, in six European countries with different climates and found that the growing season was accelerated in the hottest experimental site, with earlier emergence, flowering, and senescence than at other experimental sites. Here, we noticed that a three-degree decrease during the plant cycle preceding the floral transition can imply a substantial delay in the flowering time by about 20 days, since the cumulative growing degree-days of that period were constant between the two years. Regarding the cumulative growing degree-days, according to Deuter [25], *M. sinensis* is a plant that will flower upon an accumulation of a certain number of degree days, which was verified with our population. But our experiment did not allow for the testing of an additional effect of photoperiod on the flowering time in *M. sinensis*.

This highlights the importance of the emergence to floral transition period in explaining differences in earliness/lateness from one year to another. In particular, the differences in temperature indicators observed during that period contributed to the year effect on the flowering time in the *M. sinensis* population observed in the present study. This involved a substantial delay in the flowering time, moreover within the same site, as observed here.

The genotype × climate variances were greater than the genotype × age variances for all flowering-time related traits, which implied a decrease in the genetic parameters

In the present study, we modelled the age effect (model 1) and the climate effect (model 2) and the corresponding interaction effects on genotypes, using a staggered-start design. In both modelling processes, the spatial effects were adjusted and contributed to obtain more accurate estimates of the traits by decreasing the residual term. In all cases and for all flowering-time related traits, the genetic variance contributed to the largest part of the variance, which implied rather high heritability levels (broad-sense heritability above 0.55 and progeny-mean heritability above 0.77). Interestingly, the variance due to the genotype × climate interaction was much greater than that of the variance due to the genotype × age interaction (observed for the 4 − 3 year and the 5 − 4 year ages), thus highlighting the efficiency of the experimental staggered-start design in dividing the year effect into age and climate effects. Therefore, the climate not only implied a delay in the flowering time but also involved the differential behaviors of the genotypes, which led to higher genotype × climate interaction variances and consequently lower genetic parameters (genetic variances and heritability) for all flowering-time related traits.

Such an environmental influence on phenotypic traits has also been reported in previous studies. Clark et al. [35] estimated the heritability of 569 *M. sinensis* genotypes and 9 *M. × giganteus* for 14 yield component traits at six experimental sites, respectively. They found that the heritability estimates for the same trait were significantly different across experimental sites due to different environmental conditions. But in the present study, we also highlighted such environmental effect in a single location. Hazard et al. [36] observed that perennial ryegrass established under outdoor conditions had lower heritability estimates than ryegrass grown in greenhouses, and they suggested that the different temperature conditions during the growth processes may result in heritability changes. Regarding the year effect, Gifford et al. [19] estimated the

heritability of 13 phenotypic traits associated with biomass productivity for 221 *M. sinensis* and found an effect of the year (which includes both age and climate effects). Segura et al. [22] observed that the heritability of most architecture-related traits showed highly significant age effects by using a staggered-start design on apple trees, which was interpreted as the result of significant changes in climatic conditions. When modelling the age effect on flowering-time related traits in our study, significant changes were observed between 2018 and 2019, which can be interpreted as a result of significant different climatic conditions as well, in particular during the plant cycle prior to the floral transition.

The results above highlighted the efficiency of the staggered-start design in dissecting the year effect into age and climate effects in miscanthus. Consequently, we could observe that the genotype × climate interaction effects were much greater than the genotype × age interaction effects. Therefore, the climate not only implied a delay in the flowering time but also implied the differential behavior of the genotypes leading to higher genotype × climate interaction variances, and consequently lower genetic parameters (genetic variances and heritability). Such a result would provide further evidence that climate influences flowering-time related traits, resulting in an up to 20 % decrease in broad-sense heritability according to the flowering trait. Therefore, the breeding of such traits has to be conducted under contrasted climatic conditions in order to take into account the interactions of the genotypes with changing climate conditions.

Most flowering-time related traits of the population behaved similarly to changing climate conditions

In order to better understand the effects of climatic conditions and plant age on the flowering-time related traits in miscanthus, our study further analyzed the genetic and phenotypic correlations among all flowering-time related traits (Fig. 3). The results showed that genetic and phenotypic correlations for flowering-time related traits provided very similar information, where genetic correlation coefficients coincided with phenotypic correlation coefficients, the former being slightly larger than the latter. This indicates that the different flowering-time related traits were mainly genetically determined. Genetic correlation is a component of phenotypic correlation, and the phenotypic correlation coefficient for two traits with high genetic correlation is largely determined by the genetic correlation coefficient, which is more reliable than phenotypic correlation because genetic correlation can eliminate the influence of the environment. In this study, there were positive and strong correlations between the flowering-time related traits of SPE, AA, MPE, and CPE under the climate effect and age effect models. Interestingly, the differences in the correlation estimates were very small when comparing the climate and age models (comparison of Fig. 4a to Fig. 4c or 4d) except for the variate IHF, which corresponds to the interval between the start of panicle emergence (SPE) and that of anther appearance (AA): the lowest values were indeed obtained when the climate was modelled in comparison to the age model, and this was due to smaller genotype × age interactions than genotype × climate interactions. It seemed that all traits behaved in the same way within the population when subjected to climate condition changes, excepting the interval between the start of panicle emergence and that of anther appearance. This interval tended to be shorter under warmer conditions such those observed in 2018, and showed large differences among genotypes. Such changes according to years, regrouping age and climate effects, have been observed by Gifford et al. [19] who compared the genetic and phenotypic correlations of the two years for biomass yield, plant height, and plant circumference observed on the 221 progeny of *Miscanthus sinensis*.

Although changes in climatic conditions implied a significant delay in the flowering time and large variations in the genetic parameters of flowering-related traits, most flowering-time related traits of the population behaved similarly to varying climate conditions. The single exception was observed for the interval between the start of panicle emergence and that of anther appearance.

Conclusion And Prospects

In conclusion, the climatic conditions preceding the floral transition of *M. sinensis* led to changes in its flowering time, and temperature was one of the main variables that affected the flowering time observed on a diploid *M. sinensis* progeny. In our study, a staggered-start design was efficient in dividing the year effect into plant age and climate effects and made it possible to discover that the genotype × climate variance was much greater than the genotype × age variance for each

flowering trait. This implied that the differential behavior of genotypes led to genotype × climate interactions, which resulted in altered genetic parameters (genetic variances and heritability). In addition, most of the flowering-time related traits observed in our population - start of panicle emergence, anther appearance, mid-point of emergence, and completion of emergence - behaved similarly to changing climatic conditions, excepting the interval between the panicle emergence and anther appearance. All the results above brought strong evidence of the effect of changing climatic conditions on flowering-time related traits in *M. sinensis*, moreover observed within a single location. This resulted in non-stable earliness/lateness of the genotypes, which may impact the stability of their biomass yield itself. Therefore, breeding for flowering-time related traits in *M. sinensis* must be carried out under contrasted climatic conditions in order to consider the interaction of the genotypes with changes in climatic conditions and select more stable genotypes for the flowering time. This is critical for targeting new stable varieties, especially on marginal land where yields are known to be not only lower but highly variable. This study provides new insights for the breeding of more stable genotypes in *M. sinensis*, which is an important consideration for the cultivation of miscanthus in new areas, in particular on marginal land.

Declarations

Acknowledgements The authors gratefully acknowledge financial support from the China Scholarship Council. The authors thank the staff at the INRAE experimental unit of Estrées-Mons, GCIE Picardie, and in particular Marie-Chantal Mansard, Marie Heumez-Lévêque. We wish to thank Rebecca James who edited the English text.

Funding

The funding for this research was provided by the French National Research Agency (Agence Nationale de la Recherche, ANR), grant ANR-11-BTBR-0006-BFF in the frame of the program Investments for the Future.

Availability of data and material (data transparency)

Availability of data through GnpIS platform of INRAE: https://urgi.versailles.inra.fr/Tools/GnpIS

Authors' contributions

Maryse Brancourt-Hulmel and Wei Hou contributed to the study conception and design. Material preparation and data collection were performed by Wei Hou, Emilie Mignot and Stéphanie Arnoult. Wei Hou, Raphaël Raverdy, Catherine Giauffret and Maryse Brancourt-Hulmel contributed to data analysis. The first draft of the manuscript was written by Wei Hou and all authors commented the manuscript.

Ethics Approval and Consent to Participate

Not applicable.

Consent for Publication

All authors agree to publish this article in BioEnergy Research.

Competing Interest

The authors declare that they have no competing interests.

References

1. Gabrielle B, Bamiere L, Caldes N et al (2014) Paving the way for sustainable bioenergy in Europe: Technological options and research avenues for large-scale biomass feedstock supply. Renew Sustain ENERGY Rev 33:11–25.

https://doi.org/10.1016/j.rser.2014.01.050

2. Mohapatra S, Ray Ramesh C second, Ramachandran S third (2019) Chap. 1 - Bioethanol From Biorenewable Feedstocks: Technology, Economics, and Challenges. Bioethanol Prod Food Crops pp 3–27. https://doi.org/10.1016/B978-0-12-813766-6.00001-1
3. Lewandowski, Clifton-Brown JC, Scurlock JMO, Huisman W (2000) Miscanthus: European experience with a novel energy crop. Biomass Bioenergy 19:209–227. https://doi.org/10.1016/S0961-9534(00)00032-5
4. Linde-Laursen I (1993) Cytogenetic Analysis of Miscanthus'Giganteus', an Interspecific Hybrid. Hereditas 119:297–300. https://doi.org/10.1111/j.1601-5223.1993.00297.x
5. Hodkinson T, Chase M, Takahashi C et al (2002) The use of DNA sequencing (ITS and trnL-F), AFLP, and fluorescent in situ hybridization to study allopolyploid Miscanthus (Poaceae). Am J Bot 89:279–286. https://doi.org/10.3732/ajb.89.2.279
6. Clifton-Brown J, Hastings A, Mos M et al (2017) Progress in upscaling Miscanthus biomass production for the European bio-economy with seed-based hybrids. GCB Bioenergy 9:6–17. https://doi.org/10.1111/gcbb.12357
7. Zapater M, Catterou M, Mary B et al (2017) A Single and Robust Critical Nitrogen Dilution Curve for Miscanthus × giganteus and Miscanthus sinensis. BioEnergy Res 10:115–128. https://doi.org/10.1007/s12155-016-9781-8
8. Strullu L, Ferchaud F, Yates N et al (2015) Multisite Yield Gap Analysis of Miscanthus × giganteus Using the STICS Model. BioEnergy Res 8:1735–1749. https://doi.org/10.1007/s12155-015-9625-y
9. Clifton-Brown, Lewandowski I, Andersson B et al (2001) Performance of 15 Miscanthus Genotypes at Five Sites in Europe. Agron J 93:1013–1019. https://doi.org/10.2134/agronj2001.9351013x
10. Greef JM, Deuter M, Jung C, Schondelmaier J (1997) Genetic diversity of European Miscanthus species revealed by AFLP fingerprinting. Genet Resour Crop Evol 44:185–195. https://doi.org/10.1023/A:1008693214629
11. Głowacka K, Clark LV, Adhikari S et al (2015) Genetic variation in Miscanthus × giganteus and the importance of estimating genetic distance thresholds for differentiating clones. GCB Bioenergy 7:386–404. https://doi.org/10.1111/gcbb.12166
12. Clark LV, Brummer JE, Głowacka K et al (2014) A footprint of past climate change on the diversity and population structure of Miscanthus sinensis. Ann Bot 114:97–107. https://doi.org/10.1093/aob/mcu084
13. Clark LV, Stewart JR, Nishiwaki A et al (2015) Genetic structure of Miscanthus sinensis and Miscanthus sacchariflorus in Japan indicates a gradient of bidirectional but asymmetric introgression. J Exp Bot 66:4213–4225. https://doi.org/10.1093/jxb/eru511
14. Wagner M, Mangold A, Lask J et al (2019) Economic and environmental performance of miscanthus cultivated on marginal land for biogas production. Glob CHANGE Biol BIOENERGY 11:34–49. https://doi.org/10.1111/gcbb.12567
15. Zub HW, Brancourt-Hulmel M (2011) Agronomic and Physiological Performances of Different Species of Miscanthus, a Major Energy Crop. In: Lichtfouse E, Hamelin M, Navarrete M, Debaeke P (eds) Sustainable Agriculture Volume 2. Springer Netherlands, Dordrecht, pp 469–486
16. Clifton-Brown JC, Lewandowski I (2002) Screening Miscanthus genotypes in field trials to optimise biomass yield and quality in Southern Germany. Eur J Agron 16:97–110. https://doi.org/10.1016/S1161-0301(01)00120-4
17. Jensen E, Farrar K, Thomas-Jones S et al (2011) Characterization of flowering time diversity in Miscanthus species: FLOWERING TIME DIVERSITY IN MISCANTHUS. GCB Bioenergy 3:387–400. https://doi.org/10.1111/j.1757-1707.2011.01097.x
18. Slavov GT, Nipper R, Robson P et al (2014) Genome-wide association studies and prediction of 17 traits related to phenology, biomass and cell wall composition in the energy grass Miscanthus sinensis. New Phytol 201:1227–1239. https://doi.org/10.1111/nph.12621
19. Gifford JM, Chae WB, Swaminathan K et al (2015) Mapping the genome of *Miscanthus sinensis* for QTL associated with biomass productivity. GCB Bioenergy 7:797–810. https://doi.org/10.1111/gcbb.12201

20. Dong H, Liu S, Clark LV et al (2018) Genetic mapping of biomass yield in three interconnected Miscanthus populations. GCB Bioenergy 10:165–185. https://doi.org/10.1111/gcbb.12472
21. Loughin TM (2006) Improved Experimental Design and Analysis for Long-Term Experiments. Crop Sci 46:2492–2502. https://doi.org/10.2135/cropsci2006.04.0271
22. Segura V, Cilas C, Costes E (2008) Dissecting apple tree architecture into genetic, ontogenetic and environmental effects: mixed linear modelling of repeated spatial and temporal measures. New Phytol 178:302–314. https://doi.org/10.1111/j.1469-8137.2007.02374.x
23. Tejera M, Boersma N, Vanloocke A et al (2019) Multi-year and Multi-site Establishment of the Perennial Biomass Crop Miscanthus × giganteus Using a Staggered Start Design to Elucidate N Response. BioEnergy Res 12:471–483. https://doi.org/10.1007/s12155-019-09985-6
24. Rambaud C, Arnoult S, Bluteau A et al (2013) Shoot organogenesis in three Miscanthus species and evaluation for genetic uniformity using AFLP analysis. Plant Cell Tissue Organ Cult PCTOC 113:437–448. https://doi.org/10.1007/s11240-012-0284-9
25. Dagnelie P (2012) Principes d'Experimentation. Biometrics 38:1134. https://doi.org/10.2307/2529921
26. Warrington IJ, Kanemasu ET (1983) Corn Growth Response to Temperature and Photoperiod I. Seedling Emergence, Tassel Initiation, and Anthesis. Agron J 75:749–754. https://doi.org/10.2134/agronj1983.00021962007500050008x
27. Hesketh JD, Warrington IJ (1989) Corn Growth Response to Temperature: Rate and Duration of Lead Emergence. Agron J 81:696–701. https://doi.org/10.2134/agronj1989.00021962008100040027x
28. Munoz F, Rodriguez LS (2019) breedR: statistical methods for forest genetic resources analysis. R package version 0.12-2. Available from https://github.com/famuvie/breedR
29. Silva JCe, Dutkowski GW, Gilmour AR (2001) Analysis of early tree height in forest genetic trials is enhanced by including a spatially correlated residual. Can J For Res 31:1887–1893. https://doi.org/10.1139/x01-123
30. Gallais A (1990) Quantitative genetics of doubled haploid populations and application to the theory of line development. Genetics 124:199–206. https://www.genetics.org/content/genetics/124/1/199.full.pdf
31. Gouvêa LRL, Silva GAP, Verardi CK et al (2013) Simultaneous selection of rubber yield and girth growth in young rubber trees. Ind Crops Prod 50:39–43. https://doi.org/10.1016/j.indcrop.2013.06.040
32. Howe GT, Saruul P, Davis J, Chen THH (2000) Quantitative genetics of bud phenology, frost damage, and winter survival in an F2 family of hybrid poplars. Theor Appl Genet 101:632–642. https://doi.org/10.1007/s001220051525
33. Wei T, Simko V (2017) R package "corrplot": Visualization of a Correlation Matrix (Version 0.84). Available from https://github.com/taiyun/corrplot
34. Nunn C, Hastings AFStJ, Kalinina O et al (2017) Environmental Influences on the Growing Season Duration and Ripening of Diverse Miscanthus Germplasm Grown in Six Countries. Front Plant Sci 8:907. https://doi.org/10.3389/fpls.2017.00907
35. Clark LV, Dwiyanti MS, Anzoua KG et al (2019) Biomass yield in a genetically diverse Miscanthus sinensis germplasm panel evaluated at five locations revealed individuals with exceptional potential. GCB Bioenergy 11:1125–1145. https://doi.org/10.1111/gcbb.12606
36. Hazard L, Ghesquière M, Barraux C (1996) Genetic variability for leaf development in perennial ryegrass populations. Can J Plant Sci 76:113–118. https://doi.org/10.4141/cjps96-017

Figures

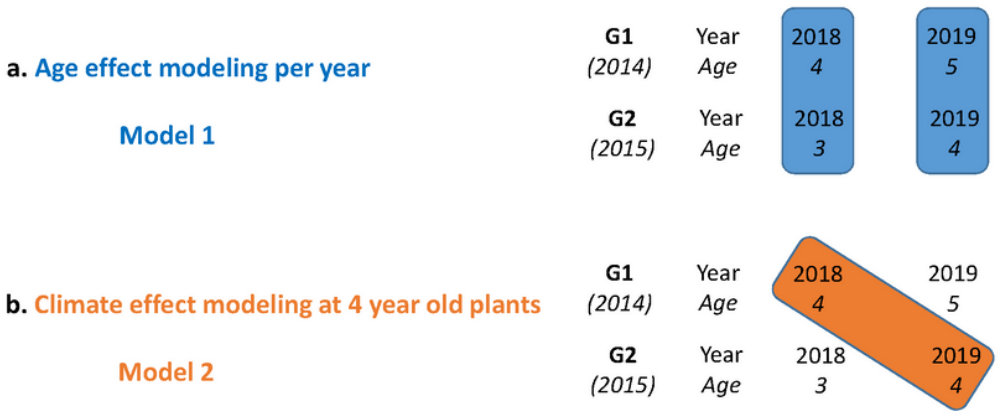

Figure 1

The staggered-start design was composed of the establishment of two groups of genotypes: G1 in 2014 and G2 in 2015. It was analyzed using an initial model which accounted for the age effect modeling per year (a) and a second model which accounted for the climate effect modeling at 4 year-old plants (b). In case (a), the year 2018 was considered for G1 and G2, with the age effect that was taken into account by 4-year old plants with G1 and 3-year old with G2. Plants of different ages grew in the same climate during a same year (2018) which makes it possible to take into account the age effect in the same climate conditions. The age effect was also analyzed in 2019 in the same manner when the genotypes were one year older. In case modeling (b), only 4-year old plants were considered: they corresponded to G1 genotypes which grew in 2018 and G2 genotypes in 2019. In this case, plants of the same age grew in two different climate conditions, related to each year considered.

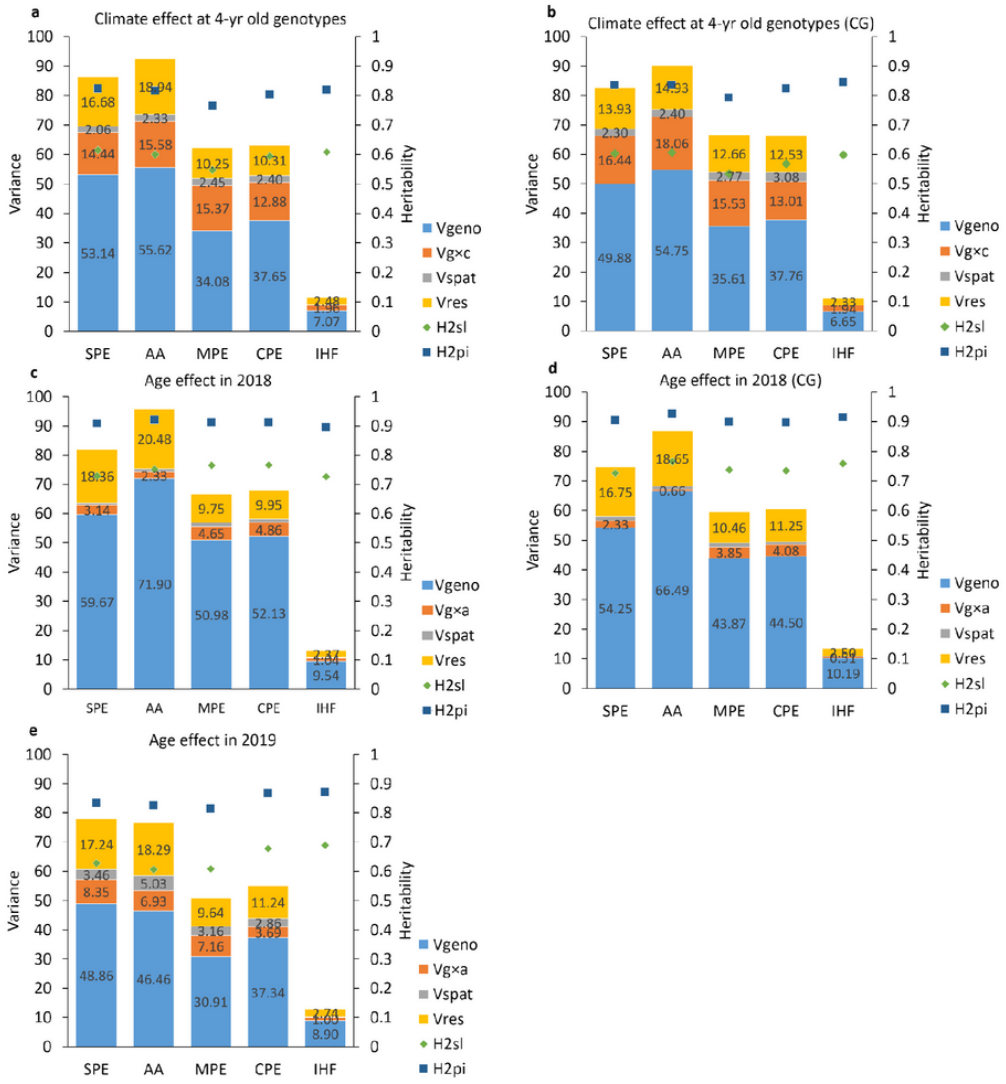

Figure 2

Estimations of genetic and environmental variances and heritability for flowering-time related traits considering age effect (model 1) or climate effect (model 2) models. The flowering-time related traits included the start of panicle emergence (SPE), anther appearance (AA), mid-point panicle emergence (MPE), complete panicle emergence (CPE), and the interval between anther appearance and the start of panicle emergence (IHF). 5 datasets were modelled: the climate effect model using the whole dataset (on a) or common genotypes between G1 and G2 (b), the age effect model observed in 2018 using the whole dataset (c) or common genotypes between G1 and G2 (d) and finally, the age effect model observed in 2019 using the whole dataset (e). Vgeno stands for genotypic variance, Vg × a for interaction variance between genotype and plant age, Vg × c for interaction variance between genotype and climate, Vspat for spatial variance and Vres for residual variance

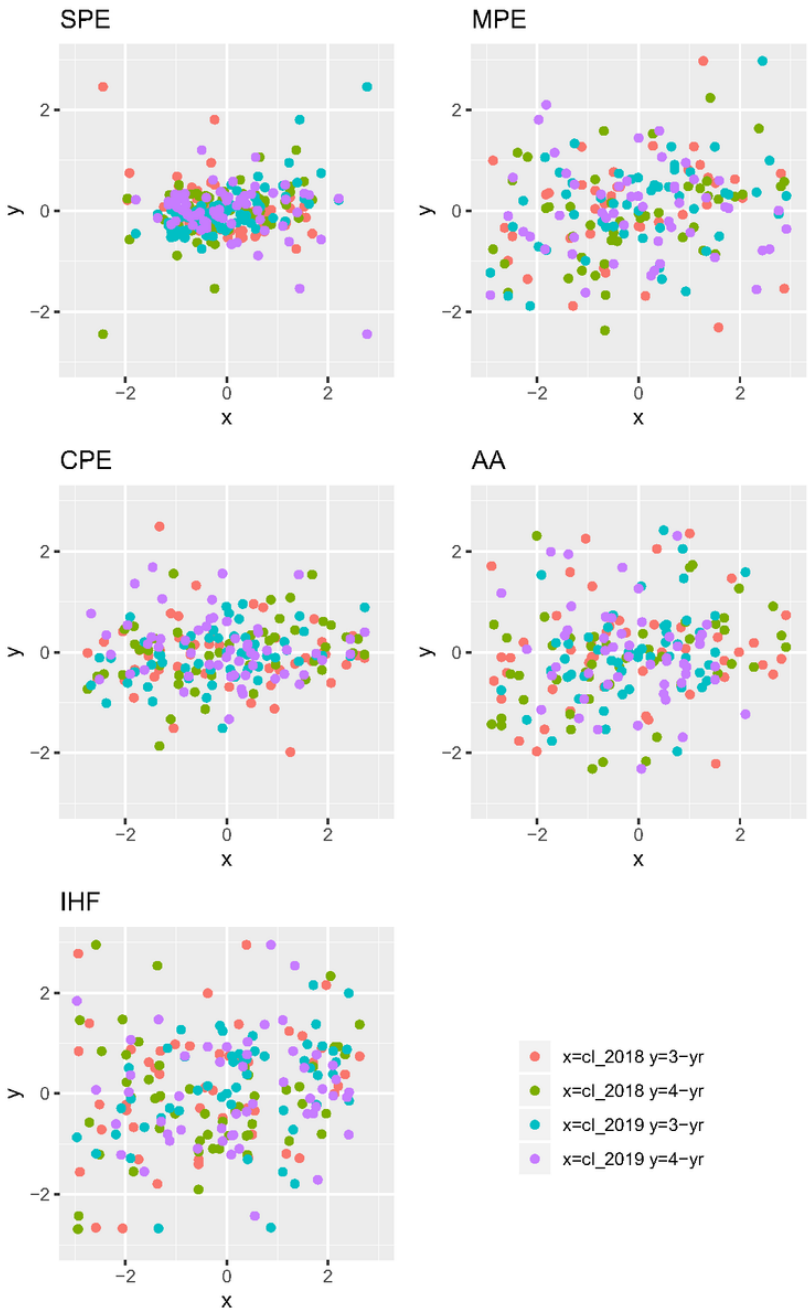

Figure 3

Illustration of the higher interactions between genotype and climate (cl_2018 and cl_2019 on the x-axis) than between genotype and age (3-yr and 4-yr on the y-axis). BLUPs of the interactions were estimated with the 82 common genotypes. The flowering-time related traits (SPE, AA, MPE, CPE, and IHF) were the same as in Fig. 2.

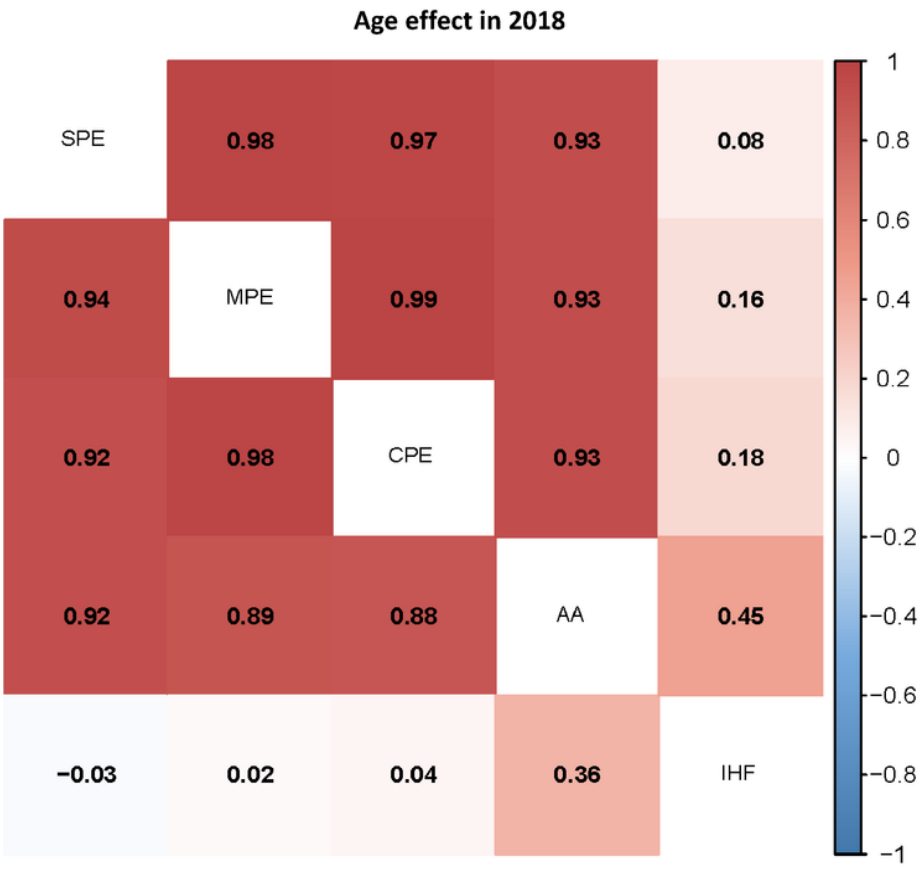

Figure 4

Phenotypic and genotypic correlation estimates among flowering-time related traits for the age effect model in 2018. The flowering-time related traits (SPE, AA, MPE, CPE, and IHF) were the same as in Fig. 2. Above the diagonal were the estimations of genotypic correlation, and below were the estimations of phenotypic correlation. Significant correlations are given at the 0.05 probability level and white cells correspond to non-significant correlations.

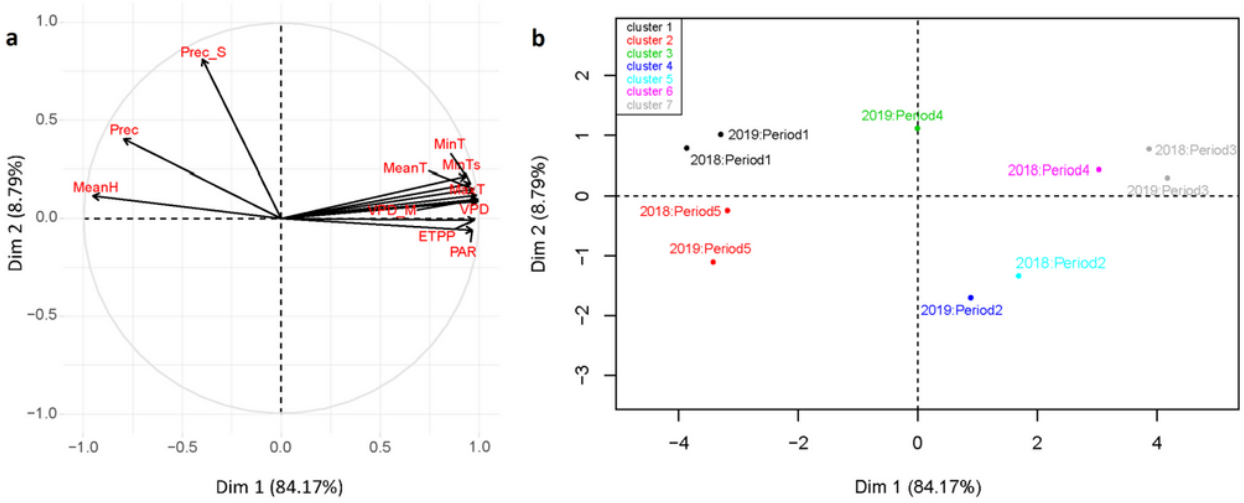

Figure 5

The principal components analysis (PCA) plot of the weather indicators according to the first and second principal components, PC1 and PC2, respectively (a). Plot illustrating the clustering of the coordinates on the first two PCA components of the individuals, i.e. 5 periods according to 2 years (b)